Evaluation of Self-Field Distributions for Bi2223 Tapes with Oxide Barriers Carrying DC Transport Current

Tomohide Makihara, Ryoji Inada, Akio Oota, Shusaku Sakamoto, Chengshan Li, and Pingxiang Zhang

***Abstract*—For AC loss reduction in Bi2223 tapes subjected to an AC external magnetic field, twisting the superconducting filaments and/or introducing oxide layers as highly resistive barriers around each filament are required. However, the structure of barrier tape becomes very complex and longitudinal uniformity of both transport property and tape structure could be easily deteriorated. To improve the current transport capability and its longitudinal uniformity for barrier tape for AC use, simple and non-destructive techniques to characterize them should be indispensable. In this paper, we examined the self-field distributions for Bi2223 tapes with oxide barriers carrying DC transport current by a scanning Hall-probe microscopy (SHM). Non-twisted and twisted 19-filamentary tapes with $SrZrO_3$ + Bi2212 barriers were prepared by powder-in-tube process. The distributions of self-field in perpendicular to the broader face of a tape carrying DC current below critical current I_c was measured at 77 K by SHM with an active area of 50 μm × 50 μm, at 0.5 mm away from the tape surface. Based on the measured self-field distributions, longitudinal non-uniformity of transport properties and the presence of local defects to obstruct the current transport in barrier tapes were investigated.**

***Index Terms*—Bi2223 tapes, oxide barriers, transport current, self-field, Hall-probe**

I. Introduction

REDUCTION of AC losses in shilver-sheathed Bi2223 tapes is one of the key issues for practical AC power devices such as transmission cables, motors and transformers. The large loss generation in an AC external magnetic field is attributed to strong electromagnetic coupling among the superconducting filaments. This interfilamentary coupling is caused by the low resistivity of pure silver matrix and/or direct connection between the filaments through interfilamentary bridging [1]. Particularly, due to geometrical anisotropy of Bi2223 tape, both hysteresis loss of superconductor and coupling loss of matrix part in a perpendicular field become much higher than in a parallel field and the conditions for filament decoupling becomes more restrictive [2], [3]. In order to achieve significant loss reduction in an AC external field with various directions against broader face of tape, therefore, not only twisting the filaments with a proper pitch length but also introducing oxide layers among the filaments as highly resistive barriers should be indispensable [4]–[8].

To date, several research works have been reported for the fabrication and characterization of Bi2223 tapes with interfilamentary oxide barriers, and noticeable loss reduction in a perpendicular field with power-grid frequency range has been already demonstrated [5]–[8]. However, the structure of a barrier tape becomes very complex and the longitudinal uniformity of both transport property and tape structure could be easily deteriorated. To improve the current transport capability and its longitudinal uniformity for barrier tape with low AC losses, simple and non-destructive techniques to characterize the locally degraded part in a tape should be strongly required.

Scanning Hall-probe Microscopy (SHM) is known to be a useful tool for magnetic and non-destructive evaluation of a variety of structural materials such as stainless steel and low carbon steel utilized in industry [9], [10]. Moreover, SHM has been also applied to characterize magnetic field distributions for Bi2223 mono- or multifilamentary tapes [11]–[15] or coated conductors [16], [17]. In this paper, we examined the self-field distributions for Bi2223 tapes with oxide barriers carrying DC transport current by SHM. Based on the experimental results, longitudinal non-uniformity of transport properties and the presence of local defects to obstruct the current transport in barrier tapes were investigated.

II. Experimental

Bi2223 tapes with interfilamentary oxide barriers were fabricated by a conventional powder-in-tube (PIT) method. $SrZrO_3$ with its mean grain size below 1 μm was selected as barrier materials because of its compatibility with Bi2223 superconductors. Moreover, additional Bi2212 powder corresponding to 15wt% was mixed with $SrZrO_3$ to improve its ductility for cold working [8]. The precursor powders were packed into pure Ag tube with an outer diameter of 9.5 mm and a wall thickness of 0.75 mm. Then, the composite was deformed into a hexagonal cross-sectional shape by drawing.

Manuscript received 3 August 2010. This work was supported in part by Grant-in-Aids for Scientific Research from MEXT(No.20686020) and JSPS (No.22560270) of Japan. It was also supported in part from TEPCO Research Foundation, Research Foundation for the Electrotechnology of Chubu (No.R-20302), DAIKO Foundation and Yazaki Memorial Foundation for Science and Technology.

T. Makihara, R. Inada, and A. Oota are with Toyohashi University of Technology, 1-1 Hibarigaoka, Tempaku-cho, Toyohashi, Aichi 4418580 Japan (e-mail: inada@ee.tut.ac.jp).

S. Sakamoto is with Kisarazu National College of Technology, 2-1-1 Kiyomidai-Higashi, Kisarazu, Chiba 2920041 Japan.

C.S. Li and P.X. Zhang are with Northwest Institute for Nonferrous Metal Research, P.O. Box 51, Xi'an Shaanxi 710016 P.R. China.

The outside surface of the monocore wire was coated by the oxide paste with the thickness of ~60 μm. After the heat treatment at 550 °C for 24 h in air to decompose and evaporate the organic binder, 19 pieces of coated monocore wire were stacked into honeycomb structure and packed into Ag-Mg alloy tube with an outer diameter of 15.5 mm and a wall thickness of 0.75 mm. The composites were drawn to a diameter of 1.83 mm and then twisted. Finally, the round wires were formed into tape shapes by flat rolling and sintered with an intermediate rolling. Typical transverse cross sectional view and specifications of barrier tapes are shown in Fig. 1 and Table 1. Cross sectional sizes and lengths for fully reacted barrier tapes are approximately 3.7 mm × 0.23 mm and 0.8–0.9 m, respectively. For comparison, the non-twisted tapes without barriers were also prepared by using same fabrication procedure.

TABLE I SPECIFICATIONS OF BI2223TAPES WITH $SrZrO_3$ + BI2212 BARRIER

Sample	T1	T2
Number of filaments	19	19
Tape cross section	3.70 mm × 0.23 mm	3.70 mm × 0.23 mm
Tape length	0.9 m	0.8 m
Twist pitch length L_t	Not twisted	10 mm
Fraction of SC filaments	24%	23%
Maximum J_c	24.6 kA/cm^2	19.2 kA/cm^2
Averaged J_c	21.2 kA/cm^2	17.3 kA/cm^2
Standard deviation of J_c	7%	9%

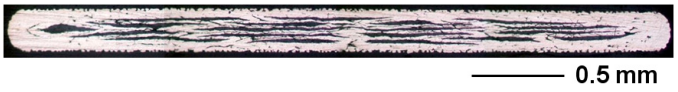

Fig. 1. Typical transverse cross sectional view of 19-filamentary Bi2223 tapes with $SrZrO_3$ + Bi2212 barriers.

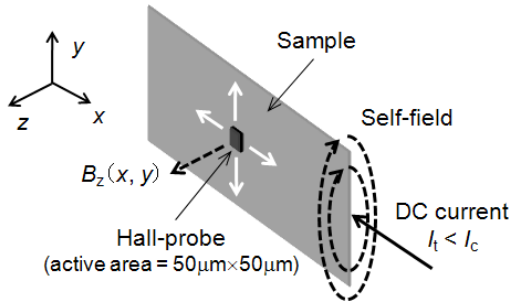

Fig. 2. A schematic diagram for measuring self-field B_z distributions on a tape by Hall-probe. The definition of coordinates is also shown. x and y directions are corresponding to longitudinal and lateral directions for the tape, respectively.

Before measuring self-field distributions, transport critical currents I_c at 77 K and self-field were measured at every 10 mm section along a length of each tape, by a conventional DC four probe method with an electric field criterion of 1 μV/cm. For I_c measurement without soldering voltage taps on a tape, contact-type voltage taps with a separation of 10 mm were used. The critical current density J_c was determined from I_c and transverse cross-sectional area of Bi2223 filaments.

Two-dimensional distributions of self-field B_z in perpendicular to the broader face of a tape carrying DC transport current $I_t < I_c$ were measured by SHM [5], [6]. Schematic diagram for self-field measurement is shown in Fig. 2. SHM was equipped with a micro-Hall probe with an active area of 50 μm × 50 μm on a movable x-y stage and a sample holder facing the probe. The probe was used to measure the magnetic field in perpendicular to the tape surface. The Hall voltages were measured using a nanovoltmeter by scanning the probe on the x-y stage with finite steps of 0.2 mm in both x- and y-directions, at a fixed distance of 0.5 mm away from a tape surface. Consequently, two-dimensional B_z distributions can be visualized in a x-y plane on a tape. The measurements were carried out at 77 K. It is noted that the time elapsed for each scan in our SHM was about 0.2 s and the scan was started right after applying DC current.

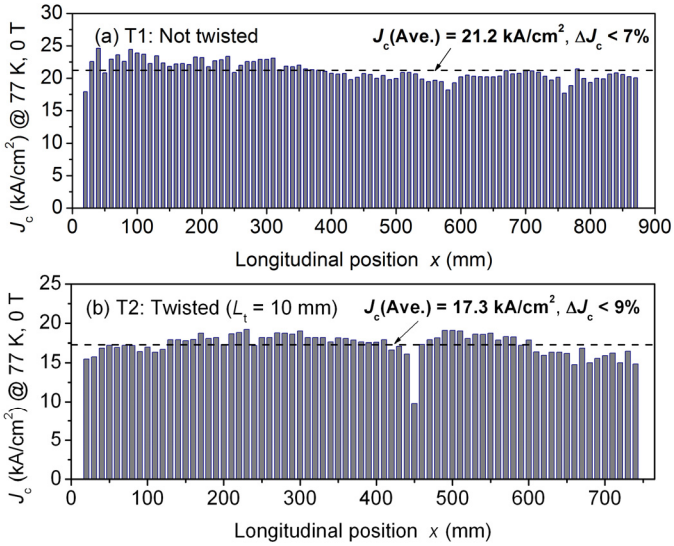

Fig. 3. Longitudinal distributions of critical current density J_c at 77 K and self-field for Bi2223 tapes with interfilamentary $SrZrO_3$ + Bi2212 barriers: (a) without twisting and (b) L_t = 10 mm. Measurements were carried out at every 10 mm section along each tape length.

III. RESULTS AND DISCUSSION

Fig. 3 shows longitudinal J_c distributions for non-twisted barrier tape T1 and twisted one T2 with L_t = 10 mm at 77 K and self-field. Maximum value, averaged value and standard deviation of J_c for each tape are also summarized in Table 1. As can be seen, averaged J_c for twisted tape T2 is approximately 20% lower than non-twisted one T1. The longitudinal uniformity of both barrier tapes was confirmed to be within 10%. Non-twisted tape T1 shows J_c > 18 kA/cm^2 in whole part along a tape length. Since averaged J_c for tapes without barriers prepared by same fabrication process was ranged in 23–24 kA/cm^2, degradation of J_c induced by introducing $SrZrO_3$ + Bi2212 barriers among the filaments was suppressed within 15%. Only for twisted barrier tape T2, sudden drop of J_c < 10 kA/cm^2 was clearly observed around x = 450 mm. In this part, generation of small transversal crack with the size of ~0.5 mm was observed in sheath part at one side of tape edge.

Based on the longitudinal J_c distribution for each tape, we measured self-field distributions at some selected regions with their section lengths of 40 mm by SHM. Fig. 4 shows two-dimensional distributions of self-field B_z in perpendicular to the wider face of non-twisted barrier tape T1 at x = 280–320

mm with higher I_c (= 47–48 A) and x = 440–480 mm with lower I_c (= 38–41 A). In both graphs, the direction of B_z is inversed at tape center (y = 0 mm) as a border and magnitude of B_z is represented by light and shade of gray color. The transport current I_t was set to be ~50% of I_c monitored at each measurement section of 40 mm. The time dependence of B_z at a specific position was checked by applying $I_t = 0.5I_c$ for several hours to confirm B_z did not vary during the measurement. This indicates that the energy dissipation with increasing time by bias current is not caused during B_z measurement. As shown in Fig. 4(a), the distribution of B_z at higher I_c section seems to be nearly uniform along a tape length so that there are no large defects to obstruct the current transport in this section. On the other hand, for lower I_c section in Fig. 4(b), the contour lines for B_z are distorted at x = 460–470 mm with the lowest I_c (= 37.8 A) part in this section. Since the lateral B_z distributions at fixed longitudinal position x are strongly influenced by field penetration inside the filamentary core of a tape, distorted contour lines of B_z at x = 460–470 mm along a tape length is attributed to the presence of locally degraded region.

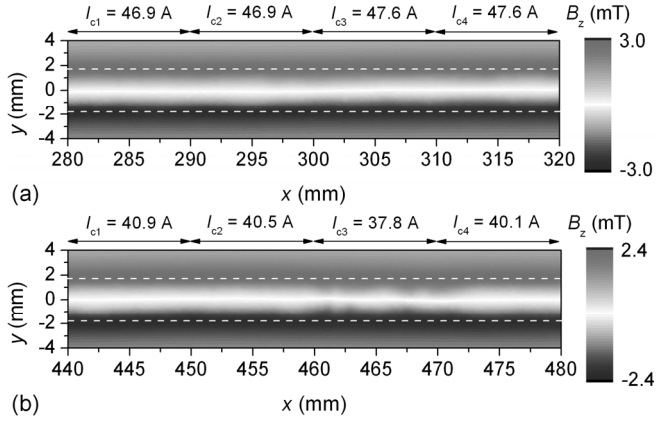

Fig. 4. Contour maps for self-field B_z on non-twisted barrier tapes T1 at (a) x = 280–320 mm with high I_c and (b) x = 440–480 mm with low I_c. White dashed lines represent the positions of both tape edges. Magnitude of transport currents I_t for each data are 24 A for (a) and 19 A for (b), respectively. Note that the direction of B_z becomes opposite at tape center (y = 0 mm) as a border.

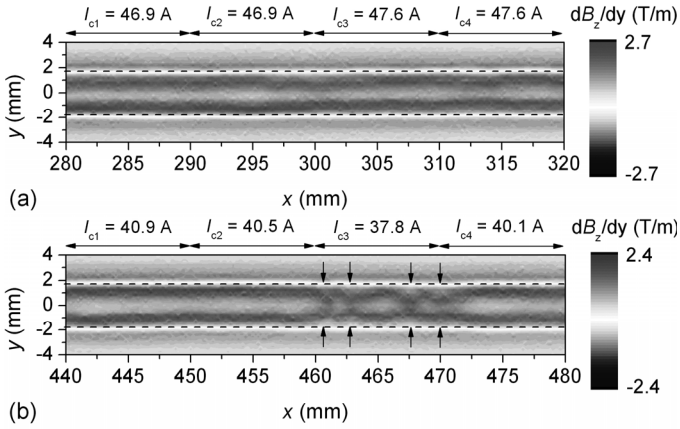

Fig. 5. Contour maps for the differentials of self-field dB_z/dy on non-twisted barrier tapes T1 at (a) x = 280–320 mm with high I_c and (b) x = 440–480 mm with low I_c. Black dashed lines represent the positions of both tape edges. Magnitude of transport currents I_t for each data are 24 A for (a) and 19 A for (b), respectively. The positions indicated by pairs of vertical arrows in (b) correspond to locally degraded region.

It is known that a differential of self-field B_z along a lateral direction dB_z/dy for a tape-form conductor strongly correlates to the sheet current density flowing in parallel to a tape length at the observation point [12], [16]. Therefore, two-dimensional distribution for dB_z/dy on a tape surface roughly corresponds to that for sheet current density. The comparison of contour maps for dB_z/dy on non-twisted barrier tape T1 at both higher and lower I_c sections are shown in Fig. 5, which is derived from the data for B_z in Fig. 4. For both measurement sections, dB_z/dy becomes larger near both tape edges, so that current is mainly flowing in outer layer of filamentary core. This behavior is consistent with conventional Bi2223 multifilamentary tapes without barriers [12], and suggests that resistive barriers among the filaments have no notable effect on self-field penetration into filamentary core under current transport. In higher I_c section at x = 280–320 mm in Fig. 5(a), the distributions for dB_z/dy along a tape length are nearly uniform. On the other hand, in lower I_c section at x = 420–460 mm in Fig. 5(b), the contour lines for dB_z/dy are distorted along a tape length at 460–470 mm with the lowest I_c (= 37.8 A). At several positions indicated by the pairs of vertical arrows, the current flowing regions from tape edges to center are more extended. At these positions, several defects were intermittently generated along a tape length during tape fabrication and current transport capability was intermittently deteriorated. We believe that such local degradation could be eliminated by optimizing the conditions for flat rolling.

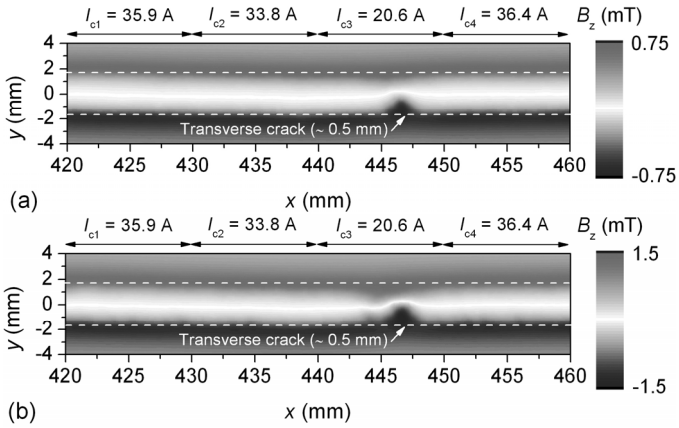

Fig. 6. Contour maps for self-field B_z on twisted barrier tapes T2 at x = 420–460 mm at (a) I_t = 5 A and (b) I_t = 10 A. White dashed lines represent the positions of both tape edges. Note that the direction of B_z becomes opposite at tape center (y = 0 mm) as a border.

The self-field B_z distribution was also evaluated for twisted barrier tape T2. Although not only barrier introduction but also filament twisting with a proper pitch length should be indispensable for reducing losses under an AC field in perpendicular to a tape face [5]–[8], filament twisting is another important factor for degrading transport property and its uniformity along a tape length [15]. Fig. 6 shows the two-dimensional B_z distribution on twisted barrier tape T2 with L_t = 10 mm at x = 420–460 mm, under different fixed transport current I_t = 5 A and 10 A. It is noted that I_c monitored at this 40 mm section was estimated to be 22 A, which is mainly determined by the lowest I_c part at x = 440–450 mm. As mentioned above, a small transversal crack with its length of

~0.5 mm at sheath part near one tape edge is observed at x = 447 mm. As can be seen, lateral field penetration is extended from both tape edges to center with increasing I_t. Near the crack position, contour lines for B_z are distorted remarkably and lateral field penetration becomes deeper than other position.

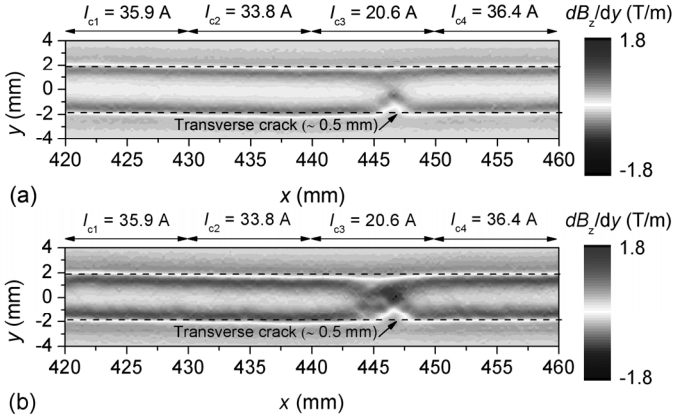

Fig. 7. Contour maps for the differentials of self-field dB_z/dy on twisted barrier tapes T2 at x = 420–460 mm at (a) I_t = 5 A and (b) I_t = 10 A. Black dashed lines represent the positions of both tape edges.

For qualitative investigation of the current distributions for twisted barrier tape T2, we also calculated dB_z/dy distribution based on B_z distribution in Fig. 6. The two-dimensional dB_z/dy distributions for tape T2 at I_t = 5 A and 10 A are shown in Fig. 7. As well as the case for non-twisted tape T1 in Fig. 5, dB_z/dy becomes larger near both tape edges at high I_c part, indicating that current is mainly flowing in outer layer of twisted filamentary core. It is also evident that the region with large dB_z/dy is extended from both tape edges to center with increasing I_t. While at x = 440–450 mm with the lowest I_c (= 20.6 A) in this measurement section, dB_z/dy shows quite complex distributions. Around x = 447 mm with a small transversal crack in sheath part, dB_z/dy becomes zero near one side of tape edge, suggesting that several filaments positioned here are damaged by the crack generation in sheath part and have no contribution for current transport. At I_t = 10 A, as shown in Fig. 7(b), dB_z/dy at x = 447 mm has the maximum near tape center so that all filaments positioned here are saturated by self-field. Although the size of crack in sheath part was not so large (~0.5 mm), its influence on local current transport capability is quite large. The processing parameters during both twisting and flat rolling must be precisely controlled to avoid such a crack generation in sheath part.

IV. Conclusion

We evaluated self-field distributions on Bi2223 tapes with interfilamentary $SrZrO_3$ + Bi2212 as resistive barriers under DC current transmission, by using a scanning Hall-probe microscopy (SHM). Non-twisted and twisted barrier tapes with their lengths of ~1 m were used for measurements. Although the longitudinal uniformity of transport J_c measured at every 10 mm sections for both tapes were within 10%, sudden drop of J_c was observed only in twisted tape. Self-field distributions on both barrier tapes are significantly distorted in lower I_c section. From the measurement for non-twisted barrier tape, it was confirmed that several defects with its longitudinal size of 1–2 mm were intermittently generated at lower I_c part. On the other hand, at the lowest I_c part in twisted tape, the filaments near one tape edge were damaged by twisting and had no contributions for current transport. Such information given by SHM has crucial importance to analyze the obstacles for current transport in barrier tape with low AC losses. In future work, we are going to examine the relations between deformation parameters during twisting and rolling process and self-field distributions systematically to improve J_c and scalability for barrier tapes.

References

[1] H.G. Knoopers, J.J. Rabbers, B. ten Haken, and H.H.J. ten Kate, "Magnetization loss in twisted multifilament Bi-2223 tape conductors," *Physica C* 372-376, pp. 1784-1787, 2002.

[2] K. Funaki, Y. Sasashige, H. Yanagida, S. Yamasaki, M. Iwakuma, N. Ayai, T. Ishida, Y. Fukumoto, and Y. Kamijo, "Development of low-AC-loss Bi-2223 superconducting multifilamentary wire," *IEEE Trans. Appl. Supercond.* 19, pp. 3053-3056, 2009.

[3] E. Martínez、Y. Yang, C. Beduz, and Y.B. Huang, "Experimental study of loss mechanisms of AgAu/PbBi-2223 tapes with twisted filaments under perpendicular AC magnetic fields at power frequencies," *Physica C* 331, pp. 216-226, 2000.

[4] K. Kwasnitza, St. Clerk, R. Flükiger, and Y.B. Huang, "Alternating magnetic field losses in high-T_c superconducting multifilament tapes with a mixed matrix of Ag and $BaZrO_3$," *Physica C* 299, pp. 113-124, 1998.

[5] K. Kwasnitza, S. Clerk, R. Flükiger, and Y. Huang, "Reduction of alternating magnetic field losses in high-Tc multifilament Bi(2223)/Ag tapes by high resistive barriers," *Cryogenics* 39, pp. 829-841, 1999.

[6] H. Eckelmann, J. Krelaus, R. Nast, and W. Goldacker, "AC losses in perpendicular external magnetic fields in ring bundle barrier multifilamentary BSCCO(2223) tapes with a central resistive barrier," *Physica C* 355, pp. 278-292, 2001.

[7] H. Eckelmann, R. Nast, C. Schmidt, and W. Goldacker, "Coupling current losses and time constants in multifilamentary BSCCO(2223) tapes with resistive barriers in external magnetic fields," IEEE Trans. Appl. Supercond. 11, pp. 2955-2958, 2001

[8] R. Inada, Y. Nakamura, A. Oota, C.S. Li, and P.X. Zhang, "Fabrication and characterization of Bi2223 tapes with interfilamentary $SrZrO_3$ + Bi2212 barriers for AC loss reduction," *Supercond. Sci. Technol.* 20, 085014, 2009.

[9] A. Oota, T. Ito, K. Kawano, D. Sugiyama, and H. Aoki, "Magnetic detection of cracks by fatigue in mild steels using a scanning Hall-sensor microscope," *Rev. Sci. Instrum.* 70, pp.184-186, 1999.

[10] A. Oota, K. Kawano, K. Miyake, T. Ito, D. Sugiyama, and H. Aoki, "Visualization of strain-induced phase breakdown in austenite stainless steel using a scanning Hall-sensor microscope," *Jpn. J. Appl. Phys.* 41, pp. 5463-5466, 2002.

[11] K. Kawano and A. Oota, "A study on self-field distribution in Ag-sheathed $(Bi,Pb)_2Sr_2Ca_2Cu_3O_x$ monofilamentary tape using a scanning Hall sensor magnetometry," *Physica C* 275, pp. 1-11, 1997.

[12] A. Oota, K. Kawano, and T. Fukunaga, "Self fields and current distribution due to DC transport currents on Ag-sheathed $(Bi,Pb)_2Sr_2Ca_2Cu_3O_x$ tapes," *Physica C* 291, pp. 188-200, 1997

[13] A. Oota, K. Kawano, and K. Yagi, "Microstructure and transport current path in Ag-sheathed $(Bi,Pb)_2Sr_2Ca_2Cu_3O_x$ monofilamentary tapes rolled at different pressures," *Ceramics International* 26, pp. 663-668, 2000.

[14] J. Kvitkovic and M. Polak, "Remanent magnetization in multifilamentary Bi-2223 tapes with filament bridging," *Physica C* 372-376, pp. 1012-1015, 2002.

[15] R. Inada, T. Makihara, Y. Araki, S. Baba, Y. Nakamura, A. Oota, S. Sakamoto, C.S. Li, and P.X. Zhang, "Non-destructive evaluation of longitudinal uniformity for twisted Bi2223 tapes using scanning Hall-probe microscopy," *Physica C* 470, pp.1392-1396, 2010.

[16] P. Usak, M. Polak, and P. Mozola, "Measurement of lateral transport current distributions in YBCO tape," *IEEE Trans. Appl. Supercond.* 19, pp. 2839-2842, 2009.

[17] M. Inoue, K. Abiru, Y. Honda, T. Kiss, Y. Iijima, K. Kakimoto, T. Saitoh, K. Nakao, and Y. Shiohara, "Observation of current distribution in high-Tc superconducting tape using scanning Hall-probe microscope," *IEEE Trans. Appl. Supercond.* 19, pp.2847-2850, 2009.